Interfacial Charge Transfer in MoS_2/TiO_2 Heterostructured Photocatalysts: The Impact of Crystal Facets and Defects

Tingcha Wei [1], Woon Ming Lau [2,*], Xiaoqiang An [3,*] and Xuelian Yu [4]

[1] Beijing Computational Science Research Center, Beijing 100193, China; wtc@csrc.ac.cn
[2] Center for Green Innovation, School of Mathematics and Physics, University of Science & Technology Beijing, Beijing 100083, China
[3] Center for Water and Ecology, State Key Joint Laboratory of Environment Simulation and Pollution Control, School of Environment, Tsinghua University, Beijing 100084, China
[4] Beijing Key Laboratory of Materials Utilization of Nonmetallic Minerals and Solid Wastes, National Laboratory of Mineral Materials, School of Materials Science and Technology, China University of Geosciences, Beijing 100083, China; xlyu@cugb.edu.cn
*   Correspondence: leolau@ustb.edu.cn (W.M.L.); xqan@tsinghua.edu.cn (X.A.)

check for updates

Abstract: One of the most challenging issues in photocatalytic hydrogen evolution is to efficiently separate photocharge carriers. Although MoS_2 loading could effectively improve the photoactivity of TiO_2, a fundamental understanding of the charge transfer process between TiO_2 and MoS_2 is still lacking. Herein, TiO_2 photocatalysts with different exposed facets were used to construct MoS_2/TiO_2 heterostructures. XPS, ESR, together with PL measurements evidenced the Type II electron transfer from MoS_2 to {001}-TiO_2. Differently, electron-rich characteristic of {101}-faceted TiO_2 were beneficial for the direct Z-scheme recombination of electrons in TiO_2 with holes in MoS_2. This synergetic effect between facet engineering and oxygen vacancies resulted in more than one order of magnitude enhanced hydrogen evolution rate. This finding revealed the elevating mechanism of constructing high-performance MoS_2/TiO_2 heterojunction based on facet and defect engineering.

Keywords: crystal facets; oxygen vacancy; molybdenum sulfide; titanium dioxide; photocatalysts; charge transfer

1. Introduction

Photocatalysis based on semiconductor nanomaterials has been extensively studied during the past decades, due to its great potential to solving the worldwide energy and environmental crisis [1,2]. Due to the abundance and high chemical stability, TiO_2 is one of the most widely used semiconductors for photocatalysis [3–5]. However, its large-scale application is seriously limited by its poor light absorption and the fast recombination of electron–hole pairs. Tremendous strategies have been used to improve the photoreactivity of TiO_2, such as morphology control, microstructure modulation, co-catalyst loading and metal/nonmetal doping [6–9]. Among these strategies, heterojunction design has proved to be the most promising way to separate photo-induced charge carriers [10,11].

MoS_2, a typical layered transition-metal dichalcogenide, attracted a lot of recent attention because of its narrow energy gap and large surface area [12–14]. Although a fundamental understanding of the heterostructured interface between TiO_2 and MoS_2 is still lacking, as-constructed junctions phenomenologically exhibited remarkably enhanced activity for photocatalytic hydrogen evolution. For example, several reports demonstrated that photo-generated electrons efficiently transferred from the conduction band of TiO_2 to MoS_2 [15–19]. The role of MoS_2 as electron reservoir renders it a

potential candidate to replace the costly noble metal cocatalysts. In contrast, several recent studies have revealed the Type II band alignment between TiO_2 and MoS_2. This meant that electrons moved from the conduction band of MoS_2 to that of TiO_2 [20–22]. This controversy was due to the fact that many factors can affect the charge transfer behavior around heterostructured interfaces. Up to now, the lithium-free fabrication of trigonal phase MoS_2 with metallic characteristic remains challenging. Ordinarily, the tunable bandgap of hexagonal phase MoS_2 (1.3–1.9 eV) unavoidably complicated the interfacial mechanism [16,23]. Moreover, the charge carrier behavior in semiconductor photocatalyst is strongly dependent on the exposed facets and structural defects. For example, {001} and {101} facets of TiO_2, two most common facets of anatase phase, usually exhibit different adsorption characteristics and redox abilities during the photocatalytic reaction [24–27]. Our research further revealed the significant contribution of facet-dependent formation of oxygen vacancy defects on the interfacial behavior of photo-induced charge carriers [28]. In this regard, it is a critical point to investigate the impact of crystal facets and defects on the charge separation in MoS_2-grafted faceted TiO_2.

In this paper, {001} and {101}-faceted TiO_2 were used to construct MoS_2/TiO_2 heterostrutures. The influence of exposed facets and oxygen vacancy defects on the interfacial separation of charge carriers was fundamentally investigated. Experimental characterizations indicated that {001} facets of TiO_2 are apt to accept electrons from MoS_2, while {101} facets are favorable for the Z-scheme recombination of electrons in TiO_2 with holes in MoS_2. The facet-dependent charge transfer process and the defect-enhanced charge separation pave a novel way to design high-efficiency heterostructured photocatalysts for energy and environmental applications.

2. Results and Discussion

Facile hydrothermal reaction was used to fabricate {001}-faceted (T001) and {101}-faceted TiO_2 (T101). Then, as-synthesized TiO_2 was heat treated under hydrogen atmosphere to obtain defective {001}-TiO_2 (V_o-T001) and {101}-TiO_2 (V_o-T101). Different types of TiO_2 was hybridized with commercial MoS_2 by ultrasonication (Figure S1). MoS_2-grafted {001}- and {101}-faceted TiO_2 without and with oxygen vacancies were denoted as T001/MoS_2, V_o-T001/MoS_2, T101/MoS_2 and V_o-T101/MoS_2, respectively.

The phase structure of as-prepared samples was examined by X-ray diffraction (XRD). As shown in Figure 1, all diffraction peaks can be indexed to anatase TiO_2 (JCPDS card No. 01-078-2486). The diffraction peaks at 25.31° and 37.79° are ascribed to (101) and (004) planes, respectively [26,29]. Thermal reduction exhibits neglectable influence on the crystal phase and crystallinity of TiO_2. No characteristic peaks of MoS_2 are discernible in the composite photocatalysts due to the relatively lower amount of MoS_2 and the high dispersity.
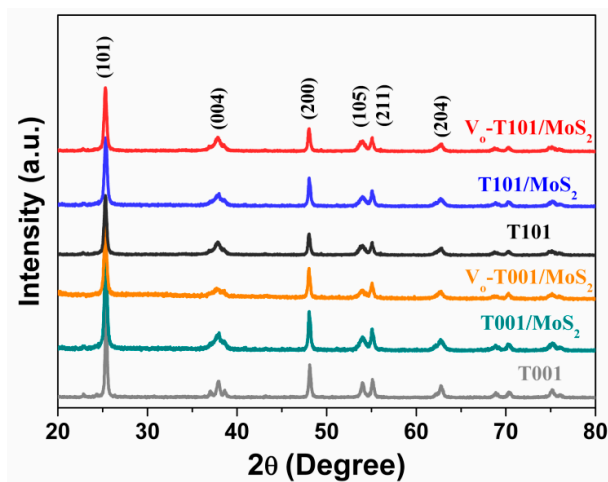
Figure 1. XRD patterns of perfect and defective faceted TiO_2 before and after the deposition of MoS_2.

Figure 2 shows the morphology of Vo-T001/MoS$_2$ and V$_o$-T101/MoS$_2$. Based on field emission scanning electron microscope (FE-SEM) and transmission electron microscope (TEM) observations, Vo-T001/MoS$_2$ sample is composed of uniform square-shaped nanosheets with an average side size of 100 nm and thickness of ~10 nm (Figure 2a,b). V$_o$-T101/MoS$_2$ sample is observed for rhombic morphology with an average apex-to-apex diameter of ~15 nm (Figure 2c,d). Figure 2e presents the high-resolution TEM image of V$_o$-T001/MoS$_2$. The lattice spacing of 0.24 nm corresponds to the (004) plane of TiO$_2$ [30]. Besides, the surface of square-shaped TiO$_2$ is intimately coupled with layered nanosheets MoS$_2$. The interlayer distance of 0.62 nm corresponds to the (002) planes of hexagonal MoS$_2$. The formation of MoS$_2$/{101}-faceted TiO$_2$ can be further confirmed by Figure 2f.
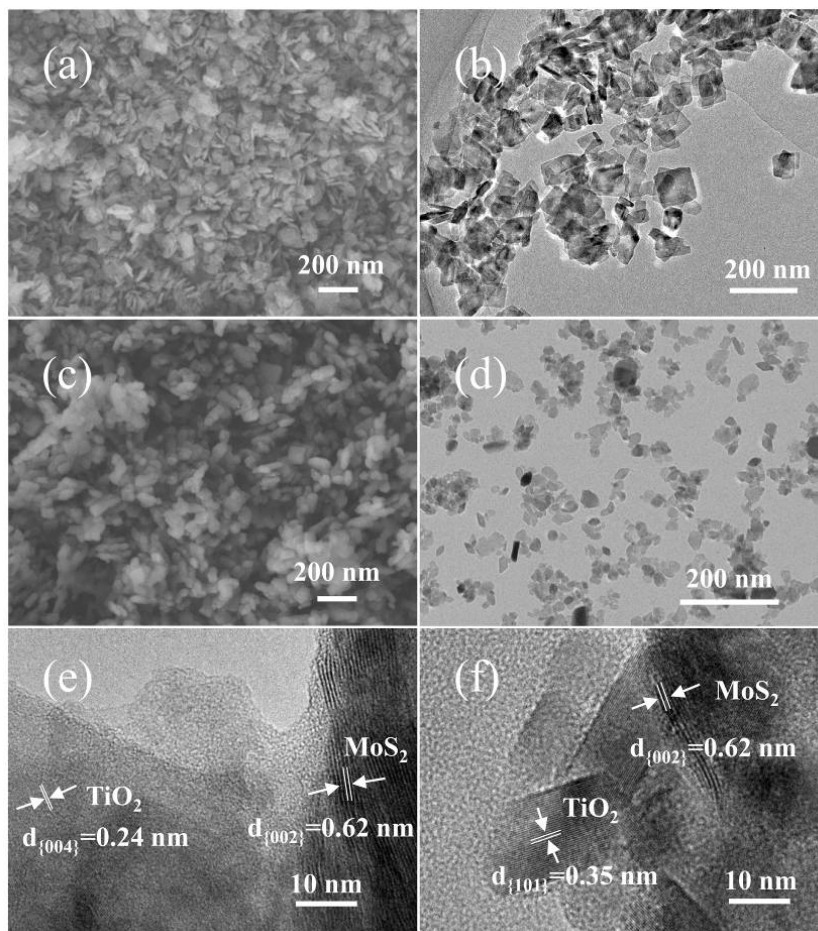
Figure 2. SEM image (**a**) and TEM image (**b**) of V$_o$-T001/MoS$_2$. SEM image (**c**) and TEM image (**d**) of V$_o$-T101/MoS$_2$. HR-TEM images of V$_o$-T001/MoS$_2$ (**e**) and V$_o$-T101/MoS$_2$ (**f**).

X-ray photoelectron spectroscopy (XPS) was used to investigate the chemical states of component elements. Figure 3a exhibits Ti 2p XPS spectra of {001}-faceted TiO$_2$, MoS$_2$/TiO$_2$ heterostructures with and without oxygen vacancies. The Ti 2p peaks shift to lower binding energies after the deposition of MoS$_2$ onto TiO$_2$ nanosheets. It means that Ti atoms accept electrons from MoS$_2$, resulting in more Ti^{3+} in the heterostructures. The creation of oxygen vacancies in TiO$_2$ further accelerates this process, as the shift value increased to 0.5 eV for V$_o$-T001/MoS$_2$. The coupling of MoS$_2$ with {101}-faced TiO$_2$ results in totally different change of spectra. The shift of Ti 2p peaks to higher binding energies indicates that Ti atom was electron donor. The facet-dependent interfacial electronic structure implies the different charge transfer behavior in T001/MoS$_2$ and T101/MoS$_2$ heterostrutures.
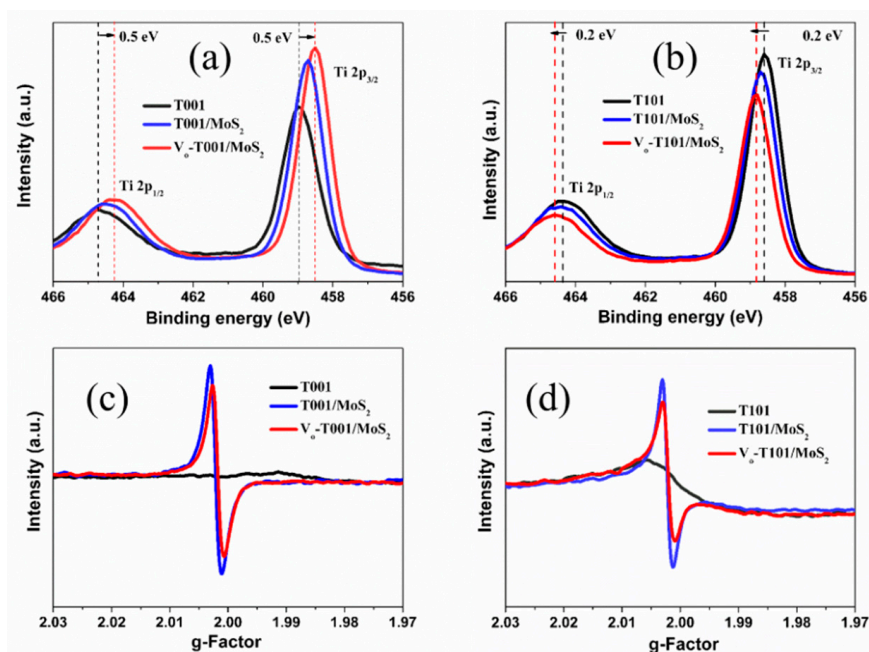
Figure 3. Ti 2p XPS spectra of {001}-faceted TiO$_2$ (**a**) and {101}-faceted TiO$_2$ (**b**) before and after the deposition of MoS$_2$ with and without defect. ESR pattern of 001-faceted TiO$_2$ (**c**) and 101-faceted TiO$_2$ (**d**) before and after the deposition of MoS$_2$ with and without defect.

The electronic structure of different samples was further studied by electron spin resonance (ESR). In Figure 3c, pristine {001}-faceted TiO$_2$ presents a weak signal around g value of 1.98–1.99, which can be ascribed to electrons trapped by Ti^{3+} [30,31]. Differently, {101}-faceted TiO$_2$ possesses a much stronger signal at 2.002 (Figure 3d). It indicates that the exposure of {101} facets is more favorable for the formation of surface oxygen vacancies [32,33]. The deposition of MoS$_2$ onto T001 and T101 results in the significantly increased ESR signals. It means that there are strong interfacial interactions between MoS$_2$ and TiO$_2$. The retention of this signal in V$_o$-T001/MoS$_2$ and V$_o$-T101/MoS$_2$ proves the formation of defective heterostructured photocatalysts.

To evaluate the influence of MoS$_2$ loading and defect formation on the light absorption ability of photocatalysts, UV-vis diffuse reflectance spectra were collected. As shown in Figure S3, {001}- and {101}-faceted TiO$_2$ only present strong absorption in the UV light region. The formation of structural defects and subsequent loading of MoS$_2$ result in the obvious visible light absorption. On the basis of Kubelka-Munk function, shown in Figure 4a,b, the corresponding band gaps of T001 and T101 are determined to be 3.06 and 2.91 eV, respectively.

In comparison, the band gap of V$_o$-T001/MoS$_2$ and V$_o$-T101/MoS$_2$ heterostructures are determined to be 2.87 and 2.74 eV, respectively. The influence of junction formation on the energy levels was investigated by valance band XPS. As shown in Figure 4c, all T001-based samples exhibit similar valence band positions, i.e. the negligible change of electronic structure. In contrast, the coupling of T101 with MoS$_2$ leads to the 0.31 eV down-shift of valence band, while the shift value decrease to 0.11 eV after the introduction of oxygen vacancies in the heterostructures (Figure 4d). All these results demonstrate the facet-dependent electronic structure in MoS$_2$/TiO$_2$ heterostructures, which should exhibit impact on the behavior of interfacial charge separation.

Photoactivity of different photocatalysts was thereafter evaluated by hydrogen evolution reactions. As show in Figure 5a, {001}-faceted TiO$_2$ exhibits moderate activity, with a hydrogen evolution rate of 20 μmol h^{-1}. After the deposition of MoS$_2$, four-fold increased photocatalytic performance is achieved. An additional 30% enhancement is achieved after the creation of oxygen vacancies in {001}-TiO$_2$. In comparison, poor photoactivity is achieved for {101}-faced TiO$_2$. The formation of T101/MoS$_2$ improves the hydrogen evolution rate from 3 μmol h^{-1} to 22 μmol h^{-1}. The formation of defective

structure presents significant impact on the photocatalytic performance. Vo-T101/MoS$_2$ possesses the highest hydrogen production rate of 61 µmol h^{-1}, which is about 20 and 3 times higher than pristine TiO$_2$ and MoS$_2$/TiO$_2$ heterojunction. The above results indicate that the construction of MoS$_2$/TiO$_2$ heterostructures can efficiently improve the photocatalytic performance of TiO$_2$. Moreover, defect modulation is a more effective strategy to improve the photoactivity of {101}-faceted TiO$_2$.
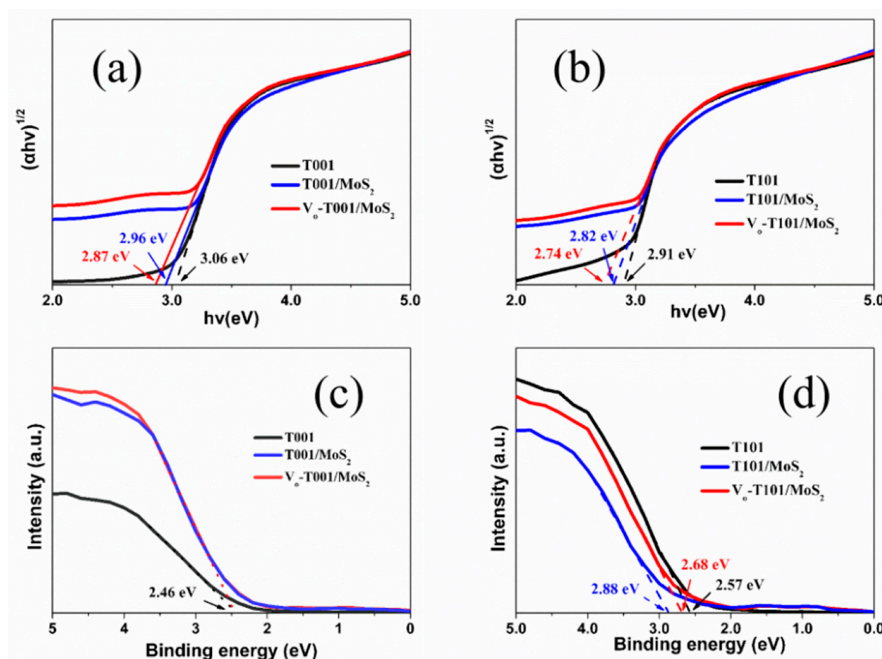
Figure 4. Tauc plots of {001}-faceted TiO$_2$ (**a**) and {101}-faceted TiO$_2$ (**b**) before and after the deposition of MoS$_2$ with and without defect. VB XPS of {001}-faceted TiO$_2$ (**c**) and {101}-faceted TiO$_2$ (**d**) before and after the deposition of MoS$_2$ with and without defects.
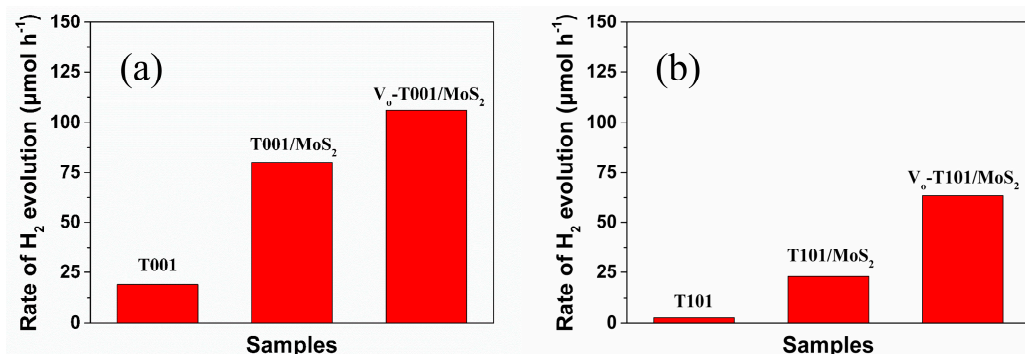
Figure 5. Photocatalytic activity of H$_2$ evolution under UV light irradiation of (**a**) {001}-faceted TiO$_2$ before and after the deposition of MoS$_2$ with and without defect and (**b**) {101}-faceted TiO$_2$ before and after the deposition of MoS$_2$ with and without defect.

In order to study the synergetic effect between oxygen vacancy defects and MoS$_2$, the charge carrier behavior was studied by photoluminescence (PL) measurements. Obviously, the deposition of MoS$_2$ and oxygen vacancy formation results in the different change of fluorescence emission of {001}- and {101}-faceted TiO$_2$.

In Figure 6a, the transition emission of T001/MoS$_2$ is much higher than pristine TiO$_2$, implying the possible electron transfer from MoS$_2$ to TiO$_2$. Differently, the formation of heterostructure and defective interface leads to the obvious PL quenching of {101}-faceted TiO$_2$ (Figure 6b) [21,34,35]. The improved separation of charge carriers can be further evidenced by the reduced radius of semi-circle in the Nyquist plots in Figure S2.
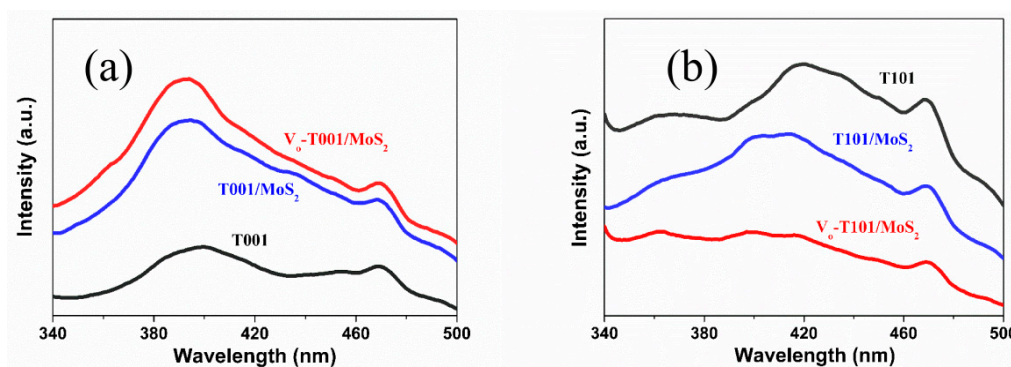
Figure 6. PL emission spectra of {001}-faceted TiO$_2$ (**a**) and {101}-faceted TiO$_2$ (**b**) before and after the deposition of MoS$_2$ with and without defect.

Based on the above results, the charge transfer mechanism in MoS$_2$-grafted faceted TiO$_2$ is illustrated in Figure 7a,b. Firstly, according to the previous reports, the purchased commercial MoS$_2$ was readily 2H-MoS$_2$ with a hexagonal structure [36,37]. Theoretically, this type MoS$_2$ in the faceted heterostructures should not be simply considered as co-catalysts for hydrogen generation. The different coordination environment of component atoms in {001}- and {101}-faceted TiO$_2$ further complicate this case. It should be noted that the amount of 5-fold-coodinated Ti on {001} facets (100%) is much larger than {101} facets (50%) of TiO$_2$ [38]. With the creation of oxygen vacancies, undercoodinated Ti4c on the surface of {001} facets can expectedly provide sufficient reactive sites for photocatalysis. However, defect modulation seemed to be more effective to improve the performance of T101/MoS$_2$ heterostructures. It indicated that this improvement was resulted from the interfacial process of charge carriers, rather than intrinsic electronic structures. Based on the UV and valence-bond XPS measurements, both the conduction band and valence band of {101}-TiO$_2$ are more positive than {001}-TiO$_2$. Therefore, more electrons should migrate to the {101} facets of TiO$_2$, while holes accumulate on the {001} facets. It means that {001}-TiO$_2$ are prone to accept electrons from MoS$_2$, i.e., the formation of Type II junction between MoS$_2$ and {001}-TiO$_2$. As shown in Figure 7a, this charge transfer process is further facilitated by the construction of defective structure. However, the deposition of MoS$_2$ onto the electron-rich {101}-TiO$_2$ results in remarkable down-shift of band gap energy levels. Its much lower conduction band is favorable for the direct recombination of these electrons with holes in the valence band of MoS$_2$, analogous to the Z-scheme mechanism [39]. When oxygen vacancies are introduced into this system, the mid-gap defect states can act as electron mediator to facilitate this charge transfer. The synergetic effect between oxygen vacancies and crystal facets leads to the more than an order of magnitude increase in hydrogen production activity.
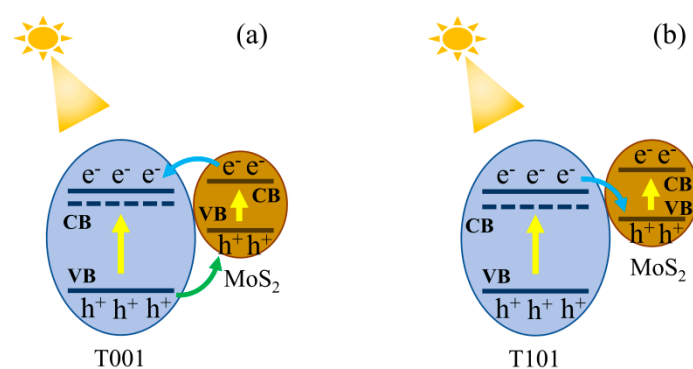
Figure 7. Scheme representation of charge separation in heterojunction for (**a**) V$_o$-T001/MoS$_2$ and (**b**) V$_o$-T101/MoS$_2$.

3. Materials and Methods

3.1. Fabrication of {001}-Faceted TiO$_2$

To fabricate {001}-faceted TiO$_2$ (T001), 1.5 mL of hydrofluoric acid was added into 12.5 mL of titanium (IV) butoxide under vigorous stirring. After 30 min, the solution was transferred into a Teflon autoclave with a capacity of 50 mL. A hydrothermal reaction was carried out at 200 °C for 24 h. When the autoclave was cooled to room temperature, the precipitants were separated by high-speed centrifugation. To remove the residual fluorine ions, the powders were soaked in 0.1 M NaOH solution for 12 h. After the fully rinsing and drying, white-colored TiO$_2$ powders were obtained, which were annealed at 400 °C for 2 h in a muffle furnace.

3.2. Fabrication of {101}-Faceted TiO$_2$

A two-step hydrothermal method was used to fabricate TiO$_2$ with exposed {101} facets (T101) [40]. In a typical procedure, 1 g of P25 TiO$_2$ nanoparticles was hydrothermally treated with 50 mL 17 M of KOH solution in a Teflon autoclave at 110 °C for 24 h. The resulting precipitates were washed and neutralized using DI water and acetic acid aqueous solution, respectively. Then the powders dried in oven for 12 h. The dried titanate powders 750 mg were further dispersed into 15 mL of ultrapure water under strong stirring. Another hydrothermal reaction was carried out at 170 °C for 24 h. Finally, the white TiO$_2$ nanoparticles were centrifuged and dried overnight. Then the powders were annealing at 400 °C for 2 h in a muffle furnace.

3.3. Synthesis of Nonstoichiometric TiO$_2$ Nanostructures

A thermal reduction strategy was used to fabricate defective TiO$_2$. Typically, as-synthesized TiO$_2$ were placed in the middle of a horizontal tube furnace. The powders were heat treated at 400 °C for 2 h in a H$_2$/Ar flow (20 mL/min).

3.4. Fabrication of MoS$_2$/TiO$_2$ Heterostructures

The fabrication procedures of MoS$_2$/TiO$_2$ heterostructure were illustrated in Scheme 1. Typically, commercial MoS$_2$ (Nanjing XFNANO Materials Tech Co., Ltd, Nanjing, China) were added into deionized water and sonicated for 8 h using ultrasonic cell disruptor (Biosafer 900-92, Nanjing Safer Biotech Co., Ltd., Nanjing, China). Then, 100 mg TiO$_2$ and a certain amount of MoS$_2$ dispersion were mixed in 50 mL of deionized water. After one hour's ultrasonication and two hours' stirring, the precipitation was filtrated, washed and dried to achieve MoS$_2$/TiO$_2$ composites. The weight ratio of MoS$_2$ in the composites was kept at 1%. All samples were prepared with the same method, using TiO$_2$ with different exposed facets and electronic structures. MoS$_2$-grafted {001}- and {101}-faceted TiO$_2$ without and with oxygen vacancies were denoted as T001/MoS$_2$, V$_o$-T001/MoS$_2$, T101/MoS$_2$ and Vo-T101/MoS$_2$, respectively.
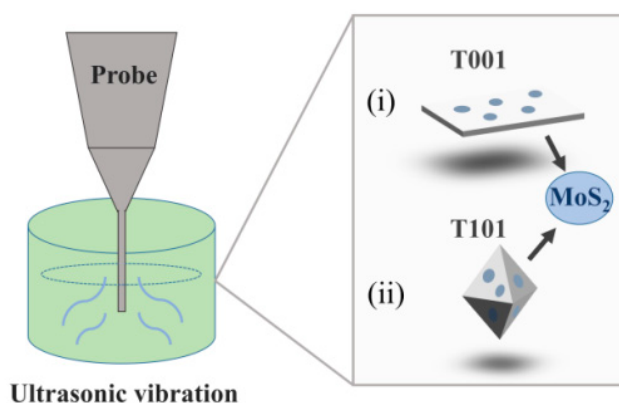
Scheme 1. Fabrication of MoS$_2$/TiO$_2$ heterostructures.

3.5. Characterizations

X-ray diffraction (XRD) was carried out on X'Pert Pro MPD (PANalytical B.V., Almelo, the Netherlands). X-ray photoelectron spectroscopy (XPS) and valence band was performed on an ESCALAB MKII spectrometer (VG Scientific Ltd., London, UK) with an Mg Kα excitation source. The morphology of catalysts were observed by field emission scanning electron microscope (FE-SEM, SIGMA, Jena, Germany) and high-resolution transmission electron microscope (HR-TEM, JEOL-2100F, JEOL, Tokyo, Japan). UV-vis diffusion reflectance spectra (DRS) were acquired on an UV−vis−NIR spectrophotometer (Cary 5000, Varian, Palo Alto, CA, USA). The steady-state fluorescence and the time-resolved fluorescence spectra were measured on a fluorescence spectrometer (FLS-980, Edinburgh Instruments Ltd., Edinburgh, UK). Electron spin resonance (ESR) analysis was carried out using a Bruker E500 spectrometer (Bruker BioSpin Gmbh, Karlsruhe, Germany).

3.6. Photocatalytic Experiments

Photocatalytic hydrogen evolution reaction was carried out in a closed gas-circulation system. Typically, 15 mg of different photocatalysts were dispersed into 100 mL aqueous solution containing 10 mL of methanol as hole scavenger. A 300 W Xe lamp (CEL-HXF300, Ceaulight, Beijing, China) was used as the light source. The evoluted H_2 was analyzed by an online gas chromatograph equipped with a column of 5 Å molecular sieves (GC-7806, Shiweipuxin, Beijing, China).

3.7. Electrochemical Measurements

The photoelectrochemical properties were investigated in a three-electrode cell using an electrochemical workstation (CHI800D, CH Instruments, Shanghai, China). The catalyst loaded FTO glass, Pt wire and Ag/AgCl electrode were used as the working electrode, counter electrode and reference electrode, respectively. 0.5 M Na_2SO_4 solution was used as electrolyte. The electrical impedance spectroscopy (EIS) was measured at an applied potential of 0 V vs. Ag/AgCl. The Mott-Schottky curves were collected at the frequency of 1000 Hz.

4. Conclusions

In summary, we have revealed that the mechanism of interfacial charge transfer in MoS_2/TiO_2 heterostructures was highly dependent with the exposed facets of TiO_2. Due to the electron-rich characteristic and the subsequent band alignment, {101} facets of TiO_2 were more favorable for the direct Z-scheme charge transfer. The introduction of oxygen vacancies into Type II heterojunction resulted in the 5-fold increased hydrogen evolution rate over MoS_2/{001}-TiO_2, while more than one order of magnitude increased activity was achieved for Z-scheme MoS_2/{101}-TiO_2. Our strategy presents a paradigm for the rational design of heterostructured photocatalysts with controlled charge transfer pathways toward photocatalytic solar energy conversion.

Supplementary Materials: The following are available online: Figure S1: TEM image of commercial MoS_2 nanosheets, Figure S2: UV-vis diffuse reflectance spectra of {001}-faceted TiO_2 (a) and {101}-faceted TiO_2 (b) before and after the deposition of MoS_2 with and without defect, Figure S3: EIS plots of {001}-faceted TiO_2 before and after the deposition of MoS_2 with and without defect.

Author Contributions: Conceptualization, W.M.L. and X.A.; Methodology, X.Y.; Formal analysis, T.W.; Investigation, W.M.L. and X.A.; Resources, X.Y.; Data curation, T.W.; Writing—original draft preparation, T.W.; Writing—review and editing, X.A.; Supervision, X.A.; Project administration, X.A.; Funding acquisition, X.A.

Conflicts of Interest: The authors declare no conflict of interest.

References

1. Wang, Q.; Hisatomi, T.; Jia, Q.; Tokudome, H.; Zhong, M.; Wang, C.; Pan, Z.; Takata, T.; Nakabayashi, M.; Shibata, N.; et al. Scalable water splitting on particulate photocatalyst sheets with a solar-to-hydrogen energy conversion efficiency exceeding 1%. *Nature Mater.* **2016**, *15*, 611–615. [CrossRef]

2. Moniz, S.J.A.; Shevlin, S.A.; Martin, D.J.; Guo, Z.-X.; Tang, J. Visible-light driven heterojunction photocatalysts for water splitting–A critical review. *Energy Environ. Sci.* **2015**, *8*, 731–759. [CrossRef]

3. Wu, L.; Li, F.; Xu, Y.; Zhang, J.W.; Zhang, D.; Li, G.; Li, H. Plasmon-induced photoelectrocatalytic activity of Au nanoparticles enhanced TiO_2 nanotube arrays electrodes for environmental remediation. *Appl. Catal. B-Environ.* **2015**, *164*, 217–224. [CrossRef]

4. Murdoch, M.; Waterhouse, G.I.N.; Nadeem, M.A.; Metson, J.B.; Keane, M.A.; Howe, R.F.; Llorca, J.; Idriss, H. The effect of gold loading and particle size on photocatalytic hydrogen production from ethanol over Au/TiO_2 nanoparticles. *Nat. Chem.* **2011**, *3*, 489–492. [CrossRef]

5. Schneider, J.; Matsuoka, M.; Takeuchi, M.; Zhang, J.; Horiuchi, Y.; Anpo, M.; Bahnemann, D.W. Understanding TiO_2 Photocatalysis: Mechanisms and Materials. *Chem. Rev.* **2014**, *114*, 9919–9986. [CrossRef] [PubMed]

6. Chen, X.; Liu, L.; Huang, F. Black titanium dioxide (TiO_2) nanomaterials. *Chem. Soc. Rev.* **2015**, *44*, 1861–1885. [CrossRef] [PubMed]

7. Li, G.; Lian, Z.; Wang, W.; Zhang, D.; Li, H. Nanotube-confinement induced size-controllable g-C_3N_4 quantum dots modified single-crystalline TiO_2 nanotube arrays for stable synergetic photoelectrocatalysis. *Nano Energy* **2016**, *19*, 446–454. [CrossRef]

8. Wang, S.L.; Luo, X.; Zhou, X.; Zhu, Y.; Chi, X.; Chen, W.; Wu, K.; Liu, Z.; Quek, S.Y.; Xu, G.Q. Fabrication and Properties of a Free-Standing Two-Dimensional Titania. *J. Am. Chem. Soc.* **2017**, *139*, 15414–15419. [CrossRef] [PubMed]

9. Zhang, K.; Wang, L.; Kim, J.K.; Ma, M.; Veerappan, G.; Lee, C.-L.; Kong, K.-J.; Lee, H.; Park, J.H. An order/disorder/water junction system for highly efficient co-catalyst-free photocatalytic hydrogen generation. *Energy Environ. Sci.* **2016**, *9*, 499–503. [CrossRef]

10. Cai, Y.; Feng, Y.P. Review on charge transfer and chemical activity of TiO_2: Mechanism and applications. *Prog. Surf. Sci.* **2016**, *91*, 183–202.

11. Gu, Q.; Long, J.; Zhuang, H.; Zhang, C.; Zhou, Y.; Wang, X. Ternary $Pt/SnO_x/TiO_2$ photocatalysts for hydrogen production: consequence of Pt sites for synergy of dual co-catalysts. *Phys. Chem. Chem. Phys.* **2014**, *16*, 12521–12534. [CrossRef]

12. Parzinger, E.; Miller, B.; Blaschke, B.; Garrido, J.A.; Ager, J.W.; Holleitner, A.; Wurstbauer, U. Photocatalytic Stability of Single- and Few-Layer MoS_2. *ACS Nano* **2015**, *9*, 11302–11309. [CrossRef] [PubMed]

13. Chang, K.; Li, M.; Wang, T.; Ouyang, S.; Li, P.; Liu, L.; Ye, J. Drastic Layer-Number-Dependent Activity Enhancement in Photocatalytic H_2 Evolution over $nMoS_2/CdS$ (n ≥ 1) Under Visible Light. *Adv. Energy Mater.* **2015**, *5*, 1402279. [CrossRef]

14. Ai, Z.; Shao, Y.; Chang, B.; Huang, B.; Wu, Y.; Hao, X. Effective orientation control of photogenerated carrier separation via rational design of a $Ti_3C_2(TiO_2)@CdS/MoS_2$ photocatalytic system. *Appl. Catal. B Environ.* **2019**, *242*, 202–208. [CrossRef]

15. Zhu, Y.; Ling, Q.; Liu, Y.; Wang, H.; Zhu, Y. Photocatalytic H_2 evolution on MoS_2–TiO_2 catalysts synthesized via mechanochemistry. *Phys. Chem. Chem. Phys.* **2015**, *17*, 933–940. [CrossRef]

16. Liu, Y.; Li, Y.; Peng, F.; Lin, Y.; Yang, S.; Zhang, S.; Wang, H.; Cao, Y.; Yu, H. 2H-and 1T-mixed phase few-layer MoS_2 as a superior to Pt co-catalyst coated on TiO_2 nanorod arrays for photocatalytic hydrogen evolution. *Appl. Catal. B Environ.* **2019**, *241*, 236–245. [CrossRef]

17. Wei, Y.; Li, L.; Fang, W.; Long, R.; Prezhdo, O.V. Weak Donor–Acceptor Interaction and Interface Polarization Define Photoexcitation Dynamics in the MoS_2/TiO_2 Composite: Time-Domain Ab Initio Simulation. *Nano Lett.* **2017**, *17*, 4038–4046. [CrossRef] [PubMed]

18. Hu, X.; Lu, S.; Tian, J.; Wei, N.; Song, X.; Wang, X.; Cui, H. The selective deposition of MoS_2 nanosheets onto (101) facets of TiO_2 nanosheets with exposed (001) facets and their enhanced photocatalytic H_2 production. *Appl. Catal. B-Environ.* **2019**, *241*, 329–337. [CrossRef]

19. Chen, B.; Meng, Y.; Sha, J.; Zhong, C.; Hu, W.; Zhao, N. Preparation of MoS_2/TiO_2 based nanocomposites for photocatalysis and rechargeable batteries: progress, challenges, and perspective. *Nanoscale* **2018**, *10*, 34–68. [CrossRef]

20. Trenczek-Zajac, A.; Banas, J.; Radecka, M. Photoactive TiO_2/MoS_2 electrode with prolonged stability. *Int. J. Hydrogen Energy* **2018**, *43*, 6824–6837. [CrossRef]

21. Mawlong, L.P.L.; Paul, K.K.; Giri, P.K. Direct CVD Growth of Monolayer MoS_2 on TiO_2 Nanorods and Evidence for Doping Induced Strong Photoluminescence Enhancement. *J. Phys. Chem. C* **2018**, *122*, 15017–15025. [CrossRef]

22. Nan, F.; Li, P.; Li, J.; Cai, T.; Ju, S.; Fang, L. Experimental and Theoretical Evidence of Enhanced Visible-light Photoelectrochemical and Photocatalytic Properties in MoS_2/TiO_2 Nanohole Arrays. *J. Phys. Chem. C* **2018**, *122*, 15055–15062. [CrossRef]

23. Chang, K.; Hai, X.; Pang, H.; Zhang, H.; Shi, L.; Liu, G.; Liu, H.; Zhao, G.; Li, M.; Ye, J. Targeted Synthesis of 2H- and 1T-Phase MoS_2 Monolayers for Catalytic Hydrogen Evolution. *Adv. Mater.* **2016**, *28*, 10033–10041. [CrossRef]

24. Xiong, Z.; Luo, Y.; Zhao, Y.; Zhang, J.; Zheng, C.; Wu, J.C.S. Synthesis, characterization and enhanced photocatalytic CO_2 reduction activity of graphene supported TiO_2 nanocrystals with coexposed {001} and {101} facets. *Phys. Chem. Chem. Phys.* **2016**, *18*, 13186–13195. [CrossRef]

25. Pan, J.; Liu, G.; Lu, G.Q.; Cheng, H.-M. On the True Photoreactivity Order of {001}, {010}, and {101} Facets of Anatase TiO_2 Crystals. *Angew. Chem.* **2011**, *123*, 2181–2185. [CrossRef]

26. Yu, J.; Low, J.; Xiao, W.; Zhou, P.; Jaroniec, M. Enhanced Photocatalytic CO_2-Reduction Activity of Anatase TiO_2 by Coexposed {001} and {101} Facets. *J. Am. Chem. Soc.* **2014**, *136*, 8839–8842. [CrossRef] [PubMed]

27. Zhou, P.; Zhang, H.; Ji, H.; Ma, W.; Chen, C.; Zhao, J. Modulating the photocatalytic redox preferences between anatase TiO_2 {001} and {101} surfaces. *Chem. Commun.* **2017**, *53*, 787–790. [CrossRef] [PubMed]

28. Wei, T.; Zhu, Y.-N.; Gu, Z.; An, X.; Liu, L.-M.; Wu, Y.; Liu, H.; Tang, J.; Qu, J. Multi-electric field modulation for photocatalytic oxygen evolution: Enhanced charge separation by coupling oxygen vacancies with faceted heterostructures. *Nano Energy* **2018**, *51*, 764–773. [CrossRef]

29. Ye, L.; Mao, J.; Liu, J.; Jiang, Z.; Peng, T.; Zan, L. Synthesis of anatase TiO_2 nanocrystals with {101}, {001} or {010} single facets of 90% level exposure and liquidphase photocatalytic reduction and oxidation activity orders. *J. Mater. Chem. A* **2013**, *1*, 10532–10537. [CrossRef]

30. Li, C.; Koenigsmann, C.; Ding, W.; Rudshteyn, B.; Yang, K.; Regan, K.; Steven, J.K.; Victor, S.B.; Gary, W.B.; Charles, A.S.; et al. Facet-Dependent Photoelectrochemical Performance of TiO_2 Nanostructures: An Experimental and Computational Study. *J. Am. Chem. Soc.* **2015**, *137*, 1520–1529. [CrossRef]

31. Qi, D.; Lu, L.; Xi, Z.; Wang, L.; Zhang, J. Enhanced photocatalytic performance of TiO_2 based on synergistic effect of Ti^{3+} self-doping and slow light effect. *Appl. Catal. B Environ.* **2014**, *160–161*, 621–628. [CrossRef]

32. Zuo, F.; Wang, L.; Wu, T.; Zhang, Z.; Borchardt, D.; Feng, P. Self-Doped Ti^{3+} Enhanced Photocatalyst for Hydrogen Production under Visible Light. *J. Am. Chem. Soc.* **2010**, *132*, 11856–11857. [CrossRef]

33. Liu, B.; Cheng, K.; Nie, S.; Zhao, X.; Yu, H.; Yu, J.; Fujishima, A.; Nakata, K. Ice–Water Quenching Induced Ti3+ Self-doped TiO_2 with Surface Lattice Distortion and the Increased Photocatalytic Activity. *J. Phys. Chem. C* **2017**, *121*, 19836–19848. [CrossRef]

34. Xu, Y.; Zhang, C.; Zhang, L.; Zhang, X.; Yao, H.; Shi, J. Pd-catalyzed instant hydrogenation of TiO_2 with enhanced photocatalytic performance. *Energy Environ. Sci.* **2016**, *9*, 2410–2417. [CrossRef]

35. Hou, Y.; Laursen, A.B.; Zhang, J.; Zhang, G.; Zhu, Y.; Wang, X.; Dahl, S.; Chorkendorff, I. Layered nanojunctions for hydrogen-evolution catalysis. *Angew. Chem.* **2013**, *52*, 3621–3625. [CrossRef]

36. Song, D.; Li, Q.; Lu, X.; Li, Y.; Li, Y.; Wang, Y.; Gao, F. Ultra-thin bimetallic alloy nanowires with porous architecture/monolayer MoS_2 nanosheet as a highly sensitive platform for the electrochemical assay of hazardous omethoate pollutant. *J. Hazard. Mater.* **2018**, *357*, 466–474. [CrossRef]

37. Shuai, C.; Sun, H.; Gao, C.; Feng, P.; Guo, W.; Yang, Y.; Zhao, M.; Yang, S.; Yuan, F.; Peng, S. Mechanical reinforcement of bioceramics scaffolds via fracture energy dissipation induced by sliding action of MoS_2 nanoplatelets. *J. Mech. Behav. Biomed. Mater.* **2017**, *75*, 423–433. [CrossRef] [PubMed]

38. Herman, G.S.; Dohnálek, Z.; Ruzycki, N.; Diebold, U. Experimental Investigation of the Interaction of Water and Methanol with Anatase-TiO_2(101). *J. Phys. Chem. B* **2003**, *107*, 2788–2795. [CrossRef]

39. Sriram, P.; Su, D.-S.; Periasamy, A.P.; Manikandan, A.; Wang, S.-W.; Chang, H.-T.; Chueh, Y.-L.; Yen, T.-J. Hybridizing Strong Quadrupole Gap Plasmons Using Optimized Nanoantennas with Bilayer MoS_2 for Excellent Photo-Electrochemical Hydrogen Evolution. *Adv. Energy Mater.* **2018**, *8*, 1801184. [CrossRef]

40. Zhang, J.; Zhou, D.; Dong, S.; Ren, N. Respective construction of Type-II and direct Z-scheme heterostructure by selectively depositing CdS on {001} and {101} facets of TiO_2 nanosheet with CDots modification: A comprehensive comparison. *J. Hazard. Mater.* **2019**, *366*, 311320. [CrossRef]

Sample Availability: Samples of the TiO2 catalysts are available from the authors.